AGU PUBLICATIONS

Water Resources Research

RESEARCH ARTICLE
10.1002/2014WR016632

Key Points:
- Fiber optic cables are inserted into the ground with direct push equipment
- Temperature is measured along vertical fiber optic cables with DTS unit
- Active heat tracer experiment is carried out to estimate groundwater velocities

Correspondence to:
M. Bakker,
mark.bakker@tudelft.nl

Citation:
Bakker, M., R. Caljé, F. Schaars, K.-J. van der Made, and S. de Haas (2015), An active heat tracer experiment to determine groundwater velocities using fiber optic cables installed with direct push equipment, *Water Resour. Res.*, *51*, 2760–2772, doi:10.1002/2014WR016632.

Received 4 NOV 2014
Accepted 17 MAR 2015
Accepted article online 1 APR 2015
Published online 26 APR 2015

An active heat tracer experiment to determine groundwater velocities using fiber optic cables installed with direct push equipment

Mark Bakker[1], Ruben Caljé[2], Frans Schaars[2], Kees-Jan van der Made[3], and Sander de Haas[4]

[1]Water Resources Section, Faculty of Civil Engineering and Geosciences, Delft University of Technology, Delft, Netherlands, [2]Artesia, Schoonhoven, Netherlands, [3]Wiertsema & Partners, Tolbert, Netherlands, [4]PWN, Heemskerk, Netherlands

Abstract A new approach is developed to insert fiber optic cables vertically into the ground with direct push equipment. Groundwater temperatures may be measured along the cables with high spatial and temporal resolution using a Distributed Temperature Sensing system. The cables may be inserted up to depths of tens of meters in unconsolidated sedimentary aquifers. The main advantages of the method are that the cables are in direct contact with the aquifer material, the disturbance of the aquifer is minor, and no borehole is needed. This cost-effective approach may be applied to both passive and active heat tracer experiments. An active heat tracer experiment was conducted to estimate horizontal groundwater velocities in a managed aquifer recharge system in the Netherlands. Six fiber optic cables and a separate heating cable were inserted with a 1 m spacing at the surface. The heating cable was turned on for 4 days and temperatures were measured during both heating and cooling of the aquifer. Temperature measurements at the heating cable alone were used to estimate the magnitude of the groundwater velocity and the thermal conductivity of the solids. The direction of the velocity and heat capacity of the solids were estimated by including temperature measurements at the other fiber optic cables in the analysis. The latter analysis suffered from the fact that the cables were not inserted exactly vertical. The three-dimensional position of the fiber optic cables must be measured for future active heat tracer experiments.

1. Introduction

The use of heat as a groundwater tracer is becoming increasingly popular in groundwater hydrology [e.g., *Anderson*, 2005]. Applications include both passive and active heat tracer experiments. In passive experiments, use is made of naturally occurring temperature variations in, for example, surface water or infiltration water [e.g., *Keery et al.*, 2007; *Rau et al.*, 2010; *Becker et al.*, 2013]. In active experiments, groundwater is either heated with a probe, or warm or cold water is injected in a borehole [e.g., *Leaf et al.*, 2012; *Ma et al.*, 2012; *Wagner et al.*, 2014]. One of the main advantages of using heat as a tracer, as compared to a solute, is that temperatures are much easier and less costly to measure than solute concentrations, especially at specific depths inside a borehole [e.g., *Ma et al.*, 2012]. One of the main complicating factors of using heat as a tracer is that heat flows through both the water and the solids, and thus depends on the thermal properties of both. Heat tracer tests and solute tracer tests commonly give similar results although several studies have reported striking differences [e.g., *Vandenbohede et al.*, 2009; *Ma et al.*, 2012; *Read et al.*, 2013].

Anderson [2005] lists a number of practical applications using heat as a groundwater tracer, including the estimation of recharge and discharge rates, hydraulic conductivity, and groundwater-surface water interaction. The application in this paper concerns the estimation of groundwater velocities. The basic concept is to raise the temperature of the groundwater at one location for a period of time and to measure the resulting temperature change through time at that same location and preferably at several other locations. Analysis of the measured temperature change at one or more locations leads to an estimate of the groundwater velocity. This approach is known as the heat pulse method in vadose zone hydrology, where the temperature change is measured with two or more temperature needles surrounding a heating needle [e.g., *Ren et al.*, 2000; *Mori et al.*, 2005]. Needles are ~3 cm long, have an outer diameter of ~2 mm, and are separated by ~6 mm; temperature is measured with thermistors. The heat pulse method is applied in the vadose

zone to estimate the water flux, water content, and thermal properties of the soil. Similar experiments are conducted in geothermics, where they are known as thermal response tests. These tests are conducted to determine the performance of borehole heat exchangers, which consist of multiple pipes installed in a grouted borehole [e.g., *Wagner et al*., 2013]. The performance, thermal properties of the aquifer, and, in some instances, the groundwater velocity, are determined from the temperature variation at the exchanger.

The estimation of the horizontal groundwater velocity in aquifers (including the variation with depth) requires heating and temperature measurements over several tens of meters in the vertical. Temperature measurements may be made over such a distance using fiber optic cables and a Distributed Temperature Sensing (DTS) system [e.g., *Selker et al*., 2006; *Tyler et al*., 2009; *van de Giesen et al*., 2012]. Application of DTS is rapidly growing in surface water hydrology [e.g., *Westhoff et al*., 2007; *Moffett et al*., 2008]. In the vadose zone, temperature is measured with DTS along horizontally placed fiber optic cables to determine soil moisture with both passive [*Steele-Dunne et al*., 2010] and active heat tracer tests [*Sayde et al*., 2010; *Striegl and Loheide*., 2012]. In the saturated subsurface, a popular application of fiber optic cables and DTS is to estimate groundwater-surface water interaction [e.g., *Lowry et al*., 2007; *Vogt et al*., 2010; *Becker et al*., 2013; *Briggs et al*., 2012; *Mamer and Lowry*, 2013]. *Hurtig et al*. [1994] reported the first groundwater application of fiber optic cables and DTS in boreholes to determine the dominant fractures and to estimate flow rates from temperature measurements. Groundwater applications in boreholes were sporadic at first [e.g., *Grosswig et al*., 1996; *Förster et al*., 1997; *Macfarlane et al*., 2002], but have picked up recently [*Freifeld et al*., 2008; *Leaf et al*., 2012; *Read et al*., 2013; *Liu et al*., 2013]. DTS has also been applied for thermal response tests in geothermics [*Fujii et al*., 2009; *Acuña et al*., 2011].

The use of boreholes for heat tracer experiments has three major drawbacks. First, boreholes are expensive to drill. Second, drilling constitutes a major disturbance of the aquifer, which effects the flow near the borehole. And third, vertical flow and exchange inside the borehole may alter the vertical distribution of the temperature. The main objective of this paper is to present a new methodology to insert fiber optic cables vertically into unconsolidated sedimentary aquifers without the need for boreholes, and to measure temperature along these cables using DTS. The methodology is used to conduct an active heat tracer test, similar to the heat pulse method in vadose zone hydrology, but on a much larger scale. Direct push equipment is used to insert fiber optic cables and a heating cable up to 20 m into the ground and approximately 1 m apart, as discussed in section 2. The field site and the heat tracer experiment are discussed in section 3 and the temperature measurements are presented in section 4. The applied mathematical model is discussed in section 5. Two methodologies to estimate groundwater velocities and several thermal properties of the soil particles are discussed in sections 6 and 7.

2. Installation of Fiber Optic Cables With Direct Push Equipment

Fiber optic cables may be inserted into the ground with direct push equipment. Direct push technology has a number of applications including the quick installation of (temporary) observation wells for hydraulic tests [*Butler et al*., 2002] and geotechnical soil investigation with cone penetration tests [e.g., *Verruijt*, 2012]. One meter long, hollow push rods are connected by a screw thread to reach the desired depth. The friction along the push rods is reduced by placing an expanded coupling behind the cone-shaped drive point. The fiber optic cable is fed through all the 1 m long push rods prior to installation. Loops of fiber optic cable are used to allow for double-ended DTS measurements. Bend-tolerable fiber optic cables must be used so that the cable can make a sharp bend at the bottom without significant disturbance of the signal. A special tool is constructed for the cone assembly. The folded middle of the fiber optic cable loop is attached to a steel drive point, which remains in the ground (see Figure 1); a short plastic protective cover fits around the bottom part of the loop and inside the push rods. The rods are pushed into the ground with a hydraulic push/pull device. When the required depth is reached, the rod assembly is retracted using the same hydraulic device. The drive point with the attached loop of fiber optic cable and protective cover remains behind in the ground and the hole collapses back around the cable.

There are four main advantages of installing fiber optic cables vertically into the ground with direct push equipment, as opposed to drilling a hole. First, the fiber optic cables are in direct contact with the groundwater and soil particles. Second, the cables may be inserted with minor disturbance of the aquifer. Third,

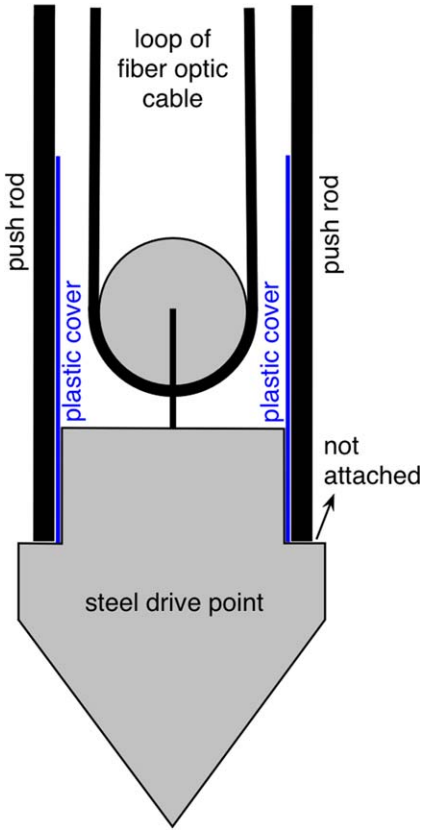

Figure 1. Schematic cross section of steel drive point, loop of fiber optic cable, and protective plastic cover that remain in the ground when the push rods are pulled back to the surface.

insertion with direct push equipment is cost effective. And fourth, installation can be combined with a cone penetration test, which provides additional and independent information about the subsurface.

3. Field Site and Heat Tracer Experiment

The proposed method of measuring groundwater temperatures along vertical fiber optic cables is tested by conducting an active heat tracer experiment at a managed aquifer recharge system in the coastal dune area near the City of Castricum in the Netherlands. The system has been operated by the drinking water company PWN to provide drinking water for the citizens of the Dutch province of North Holland since 1957. The system consists of 12 parallel elongated recharge basins and 682 recovery wells. The recharge basins are filled with pretreated surface water, which infiltrates into the shallow aquifer and flows through the dune sand to the recovery wells. Approximately 25 million cubic meters of water is infiltrated and recovered annually for the purpose of disinfection, buffering, and attenuation of water quality.

Each recharge basin is several hundred meters long, 50 m wide, and up to 2 m deep. The wells are 10 m deep with a screen ranging from 4 to 9 m below surface level (surface level is 3 m above mean sea level). The distance between the recharge basins and the recovery wells varies between 40 and 60 m. The maximum capacity of each individual well is 8 m^3/h, and the total capacity of the managed aquifer recharge system is 4500 m^3/h. The velocity of the groundwater from the recharge basin to the recovery wells is on the order of 1 m/d resulting in travel times between 21 and 60 days, which is long enough to remove all pathogens. The variation in travel times smooths out the variations in the quality of the infiltrated water.

The managed aquifer recharge system is constructed in a surficial aquifer that is approximately 38 m thick. The first 11 m consist of eolian dune sand and marine sand, followed by 12 m of silty fine sand and silty clay deposited in former beach and beach barrier environments of Holocene age. The bottom 15 m consists of coarse marine sand of Pleistocene age. The aquifer is bounded below by a 10 m thick clay layer.

The experimental equipment was installed between a recharge basin and a row of recovery wells. The layout of the experiment, including part of the recharge basin and four recovery wells is shown in Figure 2; two arrows indicate the general groundwater flow direction. Fiber optic cables are inserted close together at six locations to monitor the temperature. Locations 1–4 are spaced 1 m apart at the surface along a line approximately parallel to the flow direction. The heating cable is included at location 2 (the black dot in Figure 2). Locations 5 and 6 are 1 m to the North and South of location 3, respectively. Fiber optic cables are inserted at two additional locations: one halfway between the heat tracer experiment and the recharge basin (labeled W for West), and one halfway between the experiment and the recovery wells (labeled E for East). All cables are inserted to a depth of approximately 16 m, except at location 2, where the fiber optic cable and a heating cable are inserted to a depth of 20 m. The diameter of the fiber optic cable is 6 mm, and the diameter of the heating cable is 7 mm. The heating cable is an off-the-shelf model sold for melting

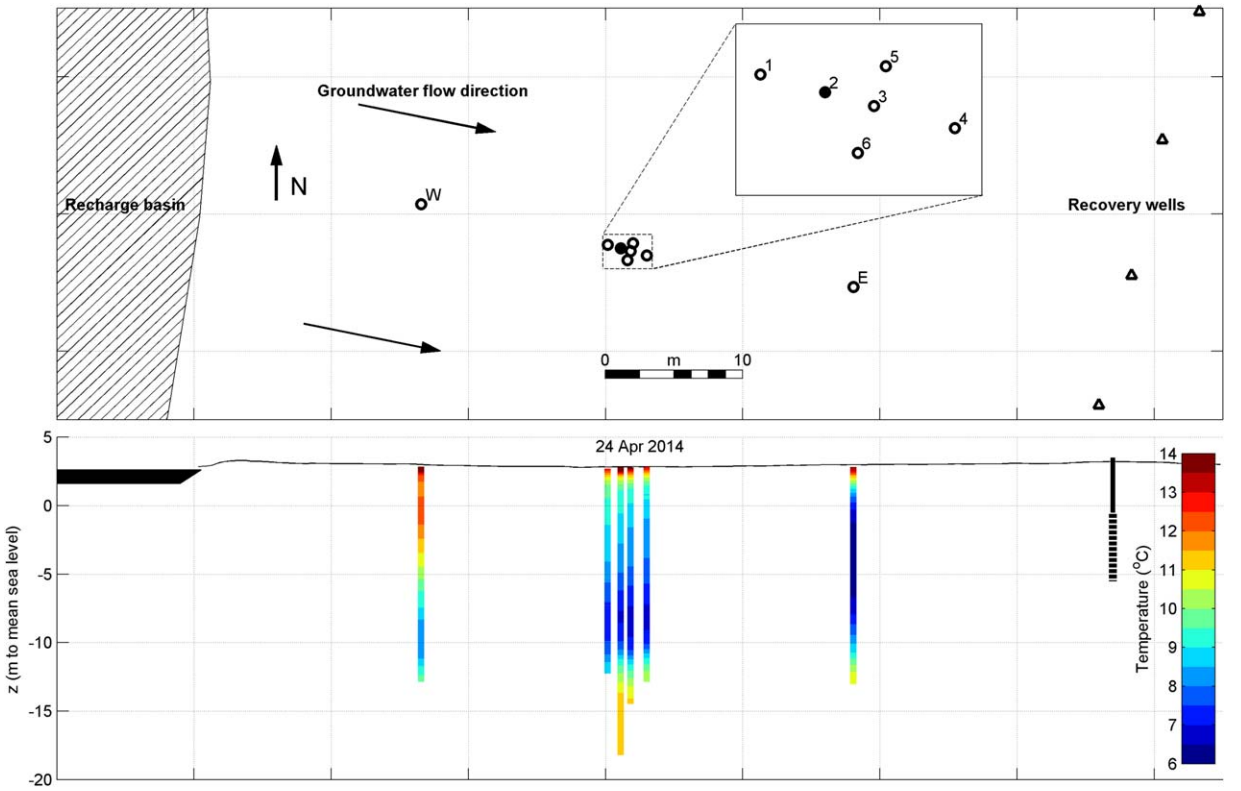

Figure 2. Layout of the (top) heat tracer experiment and (bottom) temperature measurement before start of the experiment along transect W–1–2–3–4–E. The heating cable is inserted at location 2 (black dot).

snow off drives, ramps, etc., and has a power of 30 W/m. Push rods are used with an outer diameter of 36 mm (inner diameter 16 mm), except at location 2 where the outer diameter and inner diameters are 56 mm and 39 mm, respectively, to enable installation of both the fiber optic cable and the heating cable. A cone penetration test was conducted prior to installation of the cables.

Loops of fiber optic cables were inserted such that both ends of the cable stuck out of the ground at the surface. All fiber optic cables were connected in series using a Fujikura-FSM-70S fusion splicer, resulting in one long cable that was buried underground from the measurement locations to the building with the DTS unit. No step losses were observed at the fusion splices. Warm and cold baths with separate temperature measurements were used at both ends of the cable for calibration purposes. The temperature along the fiber optic cable was measured with a Silixa Ultima DTS system, which has a sample spacing of 0.125 m and a resolution of 0.29 m.

The experiment was conducted from 24 April 2014 through 7 May 2014. The heating cable was turned on for 4 days with a power of 30 W/m. Temperature was measured every 10 min at all locations beginning an hour before the heating cable was turned on and ending 9 days after it was turned off.

4. Temperature Measurements

The initial temperature distribution on 24 April 2014 is shown along the transect W–1–2–3–4–E in the bottom half of Figure 2. The temperature varies between 14°C in the unsaturated zone above the groundwater table to 6°C around elevation $z = -8$ m at location E. The variation in temperature is due to the temporal variation of the water temperature in the recharge basin and temporal temperature variations at the surface. The vertical variation of the temperature is somewhat surprising as the temperature decreases from the surface downward, but increases again beyond a depth of ~10 m. This is likely due to the colder water that infiltrated from the recharge basin in the preceding months, the yearly temperature variation at the surface, and the smaller hydraulic conductivity of the silty fine sand below this depth. Temperature

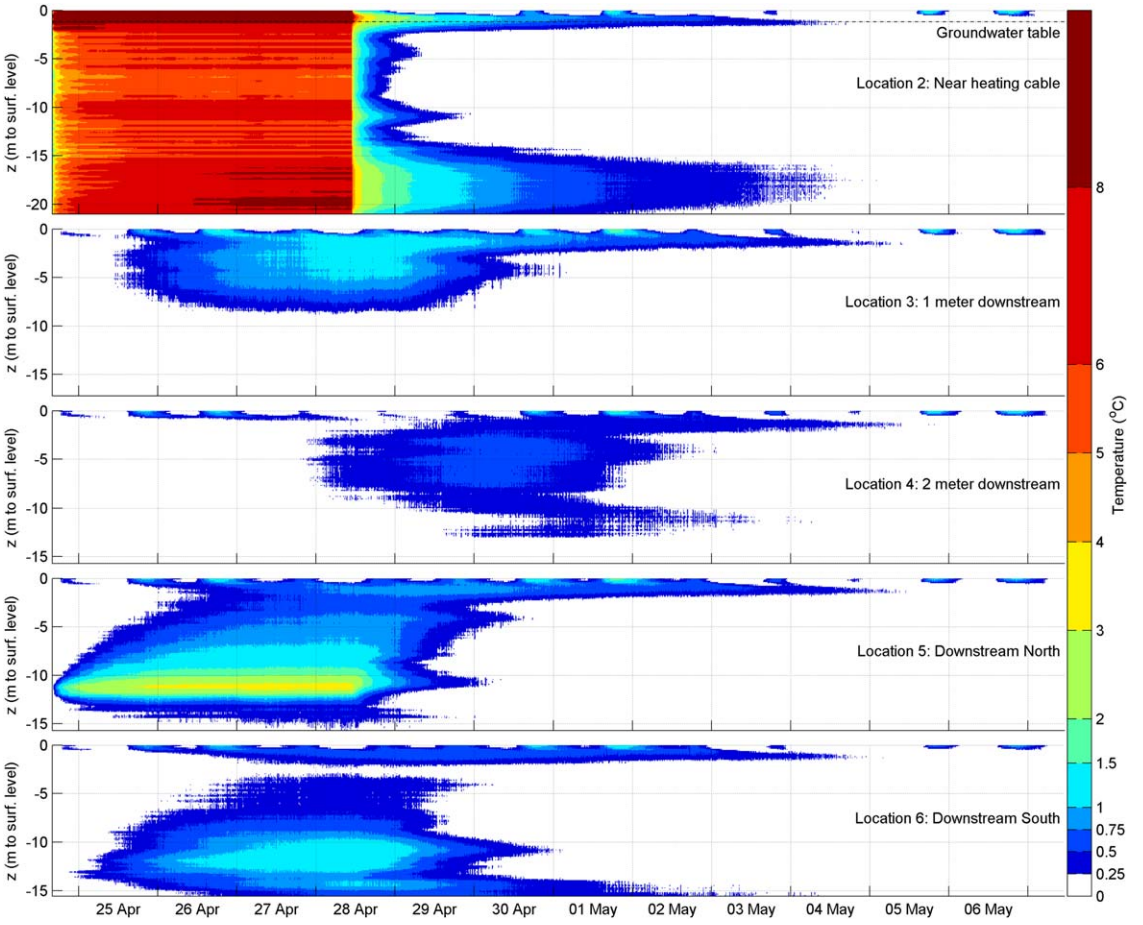

Figure 3. Temperature measurements at locations 2–6 during the active heat tracer experiment.

fluctuations due to temperature variations of the recharge basin and at the ground surface constitute a passive heat tracer test and are ongoing. The analysis of these fluctuations is beyond the scope of this paper.

The temperature changes of the groundwater that are due to past and ongoing variations in the temperature of the water in the recharge basin and at the surface are referred to as the background temperature variation. The temperature increase due to the heating cable is obtained by subtracting the background temperature from the measured temperature. The background temperature is interpolated linearly between the temperature measured before the start of the heat tracer experiment and the temperature at the end of the experiment, when all the effects of the heating cable have dissipated.

In a homogeneous sand and a homogeneous flow field, it is expected that the temperature is constant over the aquifer depth, and that the the temperature increase is smaller and arrives later at a larger distance from the heating cable. Furthermore, the temperature is expected to increase more directly downstream from the heating cable than at the same distance but in an other direction.

The measured temperature increase due to the heating cable at locations 2–6 is shown in Figure 3, where the horizontal axis is time, the vertical axis is distance to the ground surface, and the color indicates the temperature increase. The temperature increases between 5 and 8°C at the heating cable below the water table (location 2). The temperature increases significantly more than 8°C in the unsaturated zone. The temperature increase oscillates with depth at location 2. This is believed to be an artifact of the experimental setup, and is discussed in section 6. A temperature increase of 1.5°C is seen at shallow depths at location 3, 1 m downstream of the heating cable. The temperature increase is less and the temperature peak arrives later at location 4 (2 m downstream of the heating cable) than at location 3. The temperature change with depth at locations 5 and 6 does not follow the expected trend, especially at location 5, where a large

temperature increase (3–4°C) was measured at a depth of 10–12 m. Another unexpected result is that no significant temperature increase is measured at location 3 beyond a depth of ~8 m. These unexpected measurements are likely due to the fact that the fiber optic cables significantly deviate from vertical, as will be explained in section 7.

5. Mathematical Model

Groundwater flow and heat transport are approximated as two-dimensional in the horizontal *x,y* plane. The temperature of the water and solids are approximated as being at instantaneous equilibrium; thermal dispersion and buoyancy are neglected [*Anderson*, 2005]. The groundwater velocity is approximated as uniform and constant through time, and the effect of temperature on variations in density and viscosity is neglected. The two-dimensional heat transport equation for a constant and uniform groundwater velocity u in the positive x direction may be written as [e.g., *Kluitenberg and Warrick*, 2001]

$$\frac{\partial T}{\partial t} = D\left(\frac{\partial^2 T}{\partial x^2} + \frac{\partial^2 T}{\partial y^2}\right) - \frac{u}{R}\frac{\partial T}{\partial x} \tag{1}$$

where T is temperature, t is time, D is the thermal diffusivity, and R is the thermal retardation coefficient. The latter two are related to properties of the water and soil particles as follows

$$D = \frac{\kappa}{c\rho} = \frac{n\kappa_w + (1-n)\kappa_s}{nc_w\rho_w + (1-n)c_s\rho_s} \tag{2}$$

$$R = \frac{c\rho}{nc_w\rho_w} = 1 + \frac{(1-n)c_s\rho_s}{nc_w\rho_w} \tag{3}$$

where κ is the thermal conductivity, c is the mass specific heat capacity, ρ is the density, and n is the porosity. For κ, c, and ρ, the subscript s indicates the solids, the subscript w indicates water, and no subscript indicates the combined mixture of soil and water.

Consider an infinitely long vertical line source, normal to the plane of flow. The line source is located at the origin of the coordinate system and is represented in the mathematical model by a point source in the horizontal plane. The line source is heated at a constant and uniform rate q starting at time $t = t^*$. The temperature change caused by the line source starting at $t = t^*$ is Θ and may be written as [*Ren et al.*, 2000; *Kluitenberg and Warrick*, 2001]

$$\Theta(x, y, t, t^*) = \frac{q}{4\pi\kappa}\exp\left(\frac{ux}{2DR}\right)\mathrm{W}\left(\frac{x^2+y^2}{4D(t-t^*)}, \frac{u\sqrt{x^2+y^2}}{2DR}\right) \tag{4}$$

where W is the Hantush Well function defined as [e.g., *Veling and Maas*, 2010]

$$\mathrm{W}(a, b) = \int_a^\infty \frac{1}{s}\exp\left(-s - \frac{b^2}{4s}\right) ds \tag{5}$$

Equation (4) is equivalent to the moving line-source solution presented by *Zubair and Chaudhry* [1996]. The temperature due to a line source that begins heating at time t_0 and ends at time t_1 may now be written as

$$\begin{aligned} T(x, y, t) &= \Theta(x, y, t, t_0) && t_0 \le t \le t_1 \\ T(x, y, t) &= \Theta(x, y, t, t_0) - \Theta(x, y, t, t_1) && t \ge t_1 \end{aligned} \tag{6}$$

The Well function is computed through accurate numerical evaluation using adaptive Gauss-Kronrod quadrature [*Shampine*, 2008].

Typical parameters for the dune sand at the experimental site as well as the power of the heating cable (the line source) are listed in Table 1. As an example, the heating cable is turned on for 4 d, as in the field experiment, after which it is turned off. The temperature change through time is plotted for 4 locations within 1–2 cm from the heating cable plus a point 1 m downstream of the heating cable in Figure 4. The temperature increase at 1 cm from the heating cable is about 8°C after 4 days of heating and varies by 0.64°C between

Table 1. Parameter Values Used in Example of Figures 4 and 5

Specified		
n: 0.35	u: 1 m/d	q: 30 W/m
ρ_w: 1000 kg/m^3	c_w: 4100 J/kg/°C	κ_w: 0.58 W/m/°C
ρ_s: 2650 kg/m^3	c_s: 850 J/kg/°C	κ_s: 2.8 W/m/°C
Computed		
D: 0.060 m^2/d	R: 2.0	κ: 2.0 W/m/°C

locations 1 cm downstream and 1 cm upstream of the heating cable. The difference between the maximum temperature increase 1 cm downstream and 2 cm downstream of the heating cable is 1.4°C. Note that the temperature curve is significantly different for all four points near the heating cable during warming, but is very similar for all four points during cooling. This characteristic will be used to estimate the groundwater velocity in the next section. The maximum temperature increase 1 m downstream of the heating cable is almost 1.4°C, in line with the measurements at location 3 in Figure 3; the maximum is reached ∼0.6 d after the heating cable has been turned off. The maximum temperature increase 1 m upstream of the heating cable is negligible (∼0.0004°C).

Contours of the temperature change are shown in Figure 5 just before the heating cable is turned off ($t = 4$ d) and 1 day after it is turned off ($t = 5$ d). The maximum temperature in the aquifer has moved ∼0.93 m downstream of the heating cable 1 day after the heating cable is turned off.

Equation (6) is used, along with the temperature measurements during the experiment, to estimate the groundwater velocity and some of the thermal properties of the soil particles. Two analyses are presented in the next sections. In section 6, the magnitude of the groundwater velocity and the thermal conductivity of the solids are estimated from the measurements made at the heating cable only (location 2). It is known from vadose zone hydrology that the comparable single-probe heat pulse method is sensitive to the thermal conductivity and not the heat capacity [e.g., *Bristow et al*., 1994]. Similar analyses are performed to determine the thermal conductivity and the thermal resistance of the borehole in thermal response tests [e.g., *Wagner et al*., 2013]. In section 7, both the magnitude and direction of the velocity, as well as the thermal conductivity and heat capacity of the solids, are estimated based on the measurements of the temperature change at locations 2–6.

6. Analysis of the Temperature Measurements at the Heating Cable

The temperature change with depth and time at location 2 is shown in the top graph of Figure 3. The temperature change oscillates with depth in a fairly regular pattern, which is not observed at the other measurement locations. This is likely due to the installation of the cables. One loop of two fiber optic cables plus a heating cable were inserted into the ground at location 2. The three cables were taped at roughly 1 m intervals. As a result, the fiber optic cable is close to the heating cable every meter (where taped) and may be a small distance from the heating cable between the tapes. The temperature increase varies greatly over a short distance from the heating cable, as illustrated in Figure 4, where the maximum temperature increase 1 cm downstream was 1.5°C more than at 2 cm downstream. This is consistent with the vertical temperature variation measured at location 2, and hence the tape is the likely cause.

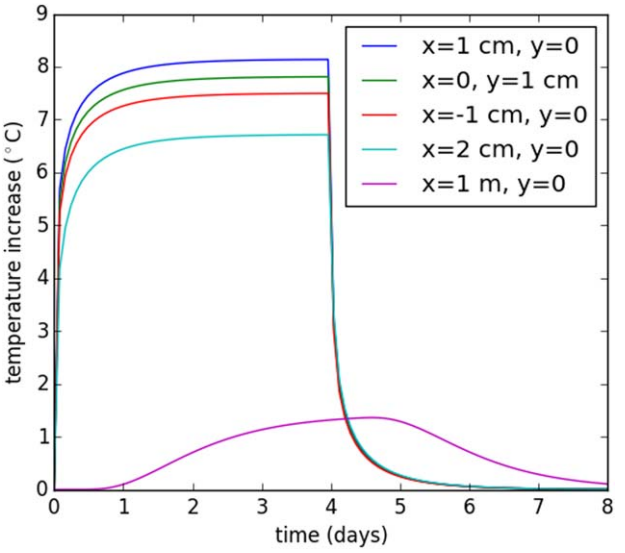

Figure 4. Temperature versus time at five locations. The heating cable is located at the origin.

It was shown in Figure 4 that the temperature variation during cooling is much less dependent on the exact location of the measurement point than during heating. Equation (6) is fitted to the measured temperature change during cooling at location 2. The magnitude of the velocity

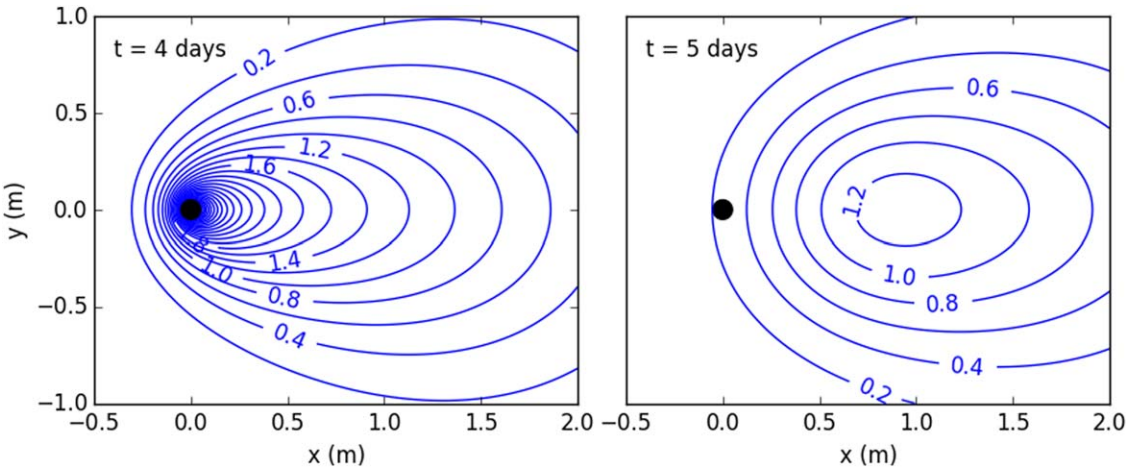

Figure 5. Contours of the temperature (°C) after (left) 4 days of heating and (right) 1 day after heating cable is turned off. The heating cable is located at the origin (black dot).

u and the thermal capacity κ_s of the solids are fitted while all other parameters are fixed to the values listed in Table 1. Optimal values of u and κ_s are estimated for each 25 cm interval by minimizing the sum of squared errors between the measured and modeled temperature change. Temperature measurements every 100 min were used for the first 2.5 days of cooling at each depth. The root mean square error was less than 0.05°C at most depths.

The estimated groundwater velocity u and thermal conductivity κ_s are shown versus depth in Figure 6. The triangles and circles in the left graph of Figure 6 represent the result of the analysis presented in the next section. Estimates for the first meter below the groundwater table are inaccurate as the mathematical model that is fitted to the data is for two-dimensional horizontal flow without vertical heat exchange. This is reasonable when the vertical temperature variation is small, but that is not the case near the water table where the temperature in the unsaturated zone is significantly different from the temperature below the water table. The correlation between u and κ_s is negative and was estimated with standard regression techniques [e.g., *Lebbe*, 1999]. Estimates of the absolute value of the correlation coefficient are less than 0.5 up to a depth of 11 m, where estimated velocities are larger than 1 m/d, and increase to 0.8–0.9 at larger depth where the velocity is less than 0.5 m/d.

The estimated velocity varies between 1 and 1.5 m/d up to a depth of 14 m, after which it decreases to less than 0.5 m/d. The variation of the friction ratio with depth, measured with a cone penetration test, is also shown in Figure 6. The value varies around 0.5 at most depths, which is indicative of sand in this area, while smaller values indicate coarser sand. Small peaks in the friction ratio (above 1) represent thin layers of silty sand in this area and are not visible in the estimated velocity, which represents average values over 25 cm intervals. The zone of larger friction ratios at a depth of 11–12 m corresponds to a zone of smaller velocity values. The friction ratio is almost consistently above 0.5 and the estimated velocity is consistently smaller than 0.5 m/d below a depth of 14 m. The fitted thermal conductivity κ_s of the solids varies in the range 3–4.5 W/m/°C with an average value of 3.6 W/m/°C, which is high for (silty) sand particles.

The fitted values for u and κ_s are dependent on the choice of the other parameter values (Table 1). For example, the fitted value of the thermal diffusivity is $D = 0.076$ m^2/d for the mean value of κ_s of 3.6 W/m/°C and the other parameter values from Table 1. The same value of D may be obtained with a slightly higher porosity $n = 0.4$ and heat capacity $c_s = 1150$ J/kg/°C while the thermal retardation increases only slightly to $R = 2.1$.

7. Analysis of the Temperature Measurements at Locations 2–6

Temperature measurements at locations 2–6 are analyzed to determine the direction of the velocity α and the mass specific heat capacity of the solids c_s in addition to the magnitude of the velocity and the thermal conductivity of the solids. The direction is measured counter-clockwise with respect to straight East.

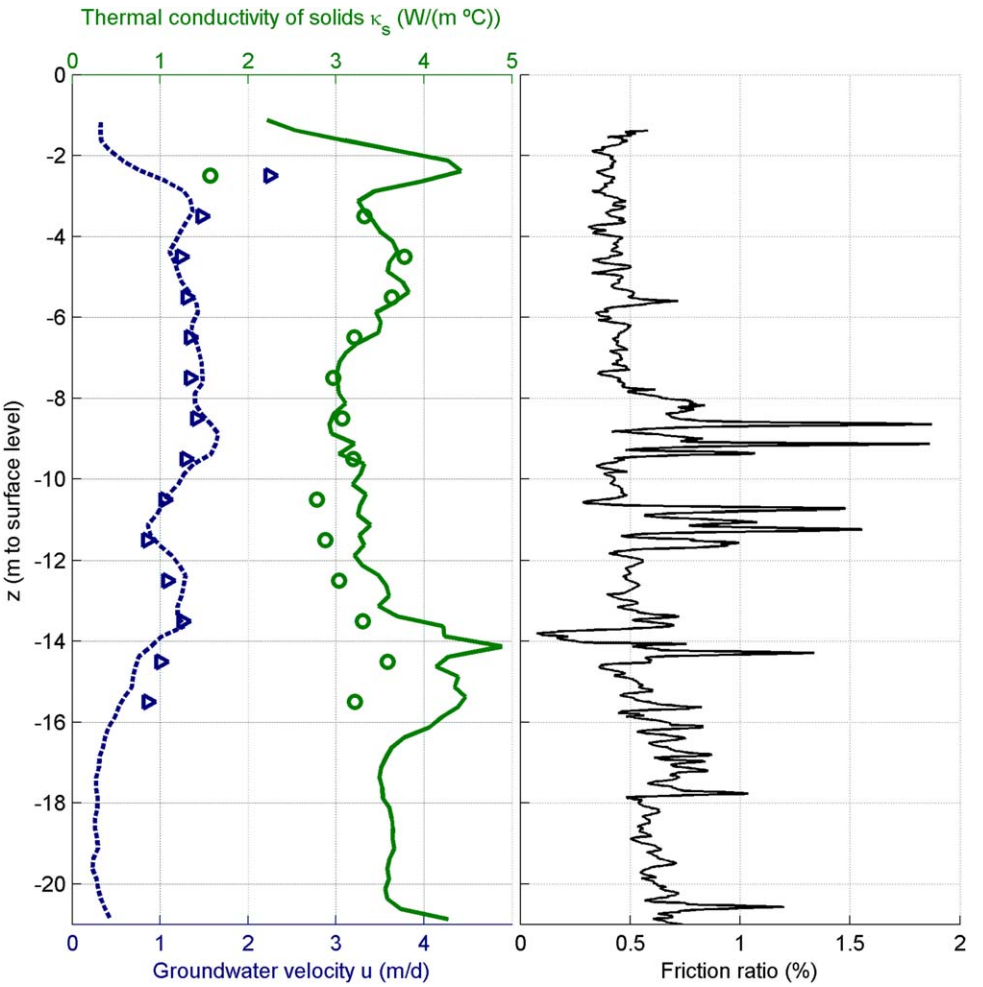

Figure 6. (left) Velocity u and thermal conductivity of the solids κ_s versus depth; lines are estimated from temperature measurements at the heating cable, triangles and circles are estimated from temperature measurements at five cables. (right) Friction ratio measured with cone penetration test.

Equation (6) was fitted to the temperature data for 14 one meter sections at locations 2–6. This gave reasonable values at shallow depths, but no reasonable match was possible at greater depth. This is no surprise, as unexpected temperature variations were observed at greater depth (Figure 3). These variations cannot be explained by variations in the rather homogeneous aquifer material or any other groundwater process. They can only be explained if it is assumed that the fiber optic cables are not inserted exactly vertically and parallel, which means that the distance and location of the cables with respect to each other varies with depth. A deviation of 1–2° from the vertical is possible when positioning the direct push truck. In addition, the steel rods may bend slightly when they are pushed into the ground. The exact paths of the steel rods may be measured, but this was not done during installation (more on that in section 8).

The approximate position of the cables at locations 3–6 relative to the cable at location 2 was determined by assuming that each cable was straight and inserted with a constant angular deviation from the vertical and from the horizontal. All other parameters were fixed to the values of Table 1. Eight different angles (two for each cable) were fitted simultaneously by minimizing the sum of squared errors between the measured and modeled temperature change. After the optimal angles were determined, the optimal values for the thermal conductivity and heat capacity of the solids, as well as the magnitude and orientation of the horizontal velocity were determined by fixing the angles and using the values for all other parameters from Table 1. Values were estimated for 14 one meter intervals by minimizing the sum of squared errors between the modeled and measured temperature change over 4 days of heating and 3 days of cooling; measured

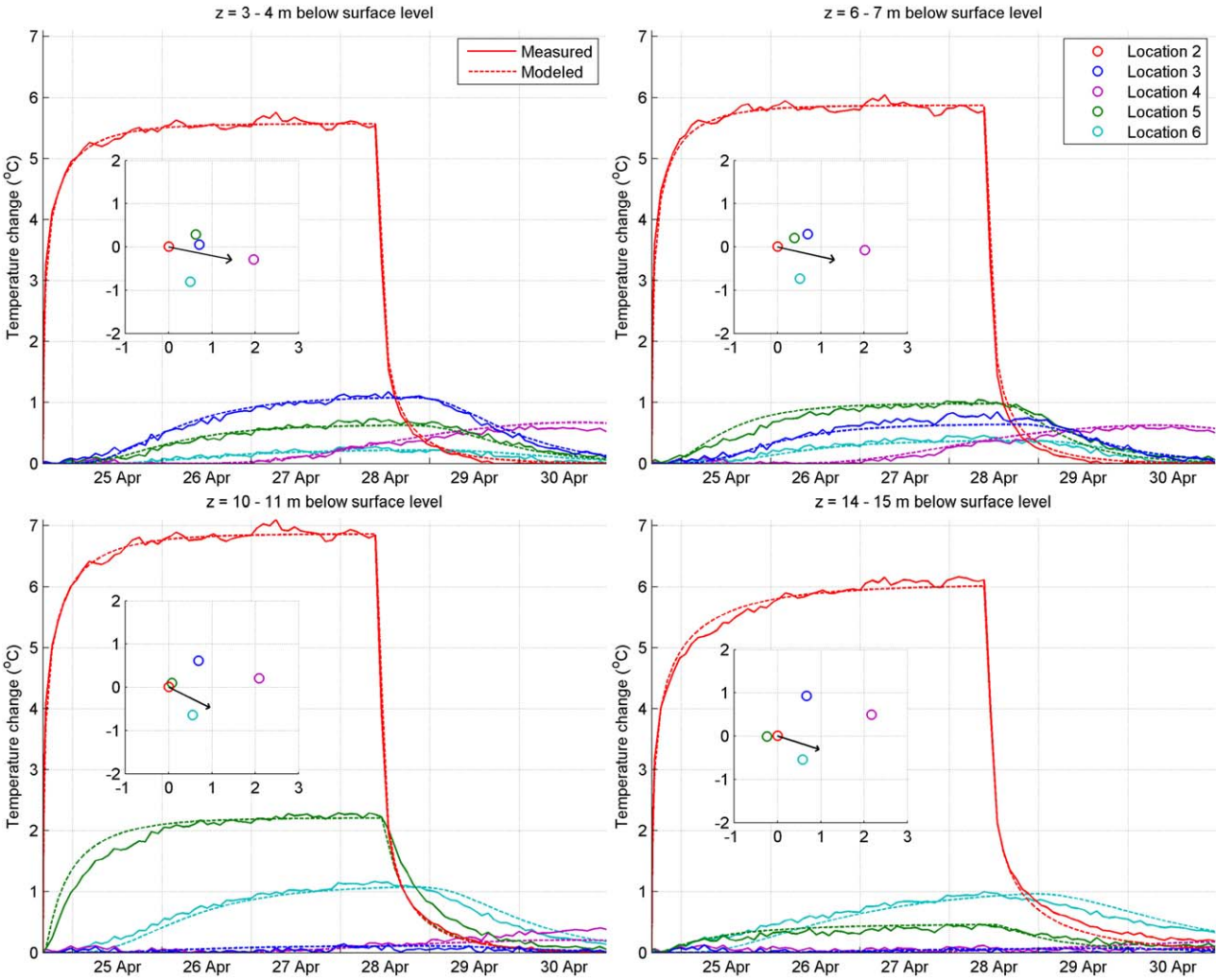

Figure 7. Fit between the measured (solid) and modeled (dotted) temperature variation at four depths for locations 2–6. The insert shows the location of the fiber optic cables at the respective depths. The arrow in the insert represents the fitted velocity vector.

temperatures were averaged for each 1 m interval. The fit is shown for four depth intervals in Figure 7. The little inserts in the graphs show the estimated locations of the five cables relative to each other at the depth shown. The arrow represents the fitted groundwater velocity. At shallow depth (3–4 m), the fiber optic cables are near the location layed out at the surface (Figure 2). Cable 3 angles to the North, which explains why almost no temperature increase was measured along this cable at larger depth. Cable 5 angles to the southwest and approaches cable 2 at a depth of 10–11 m, which explains the observed temperature increase at this depth (Figure 3). At larger depth (14–15 m), cable 5 is even slightly upstream of cable 2.

The fitted values of all four parameters are plotted versus depth in Figure 8 (black line). The values at a depth of 2–3 m, right below the water table, are inaccurate, as for the analysis in section 6, and should be neglected. The magnitude of the velocity varies roughly in the range 1–1.5 m/d. The angle representing the direction of the velocity varies over a range of 20° from −11° at a depth of 3–4 m to −26° at a depth of 10–11 m and then back to −6° at a depth of 15–16 m. The thermal conductivity varies over a reasonable range (2.8–3.8 W/m/°C). The estimated heat capacity varies over an unrealistically large range (500–1500 J/kg/°C) while the mean (1060 J/kg/°C) is reasonable for silty sand. The corresponding thermal diffusivity varies between 0.046 and 0.092 m^2/d with a mean of 0.064 m^2/d. The corresponding thermal retardation coefficient varies between 1.4 and 3.0 with a mean of 2.3.

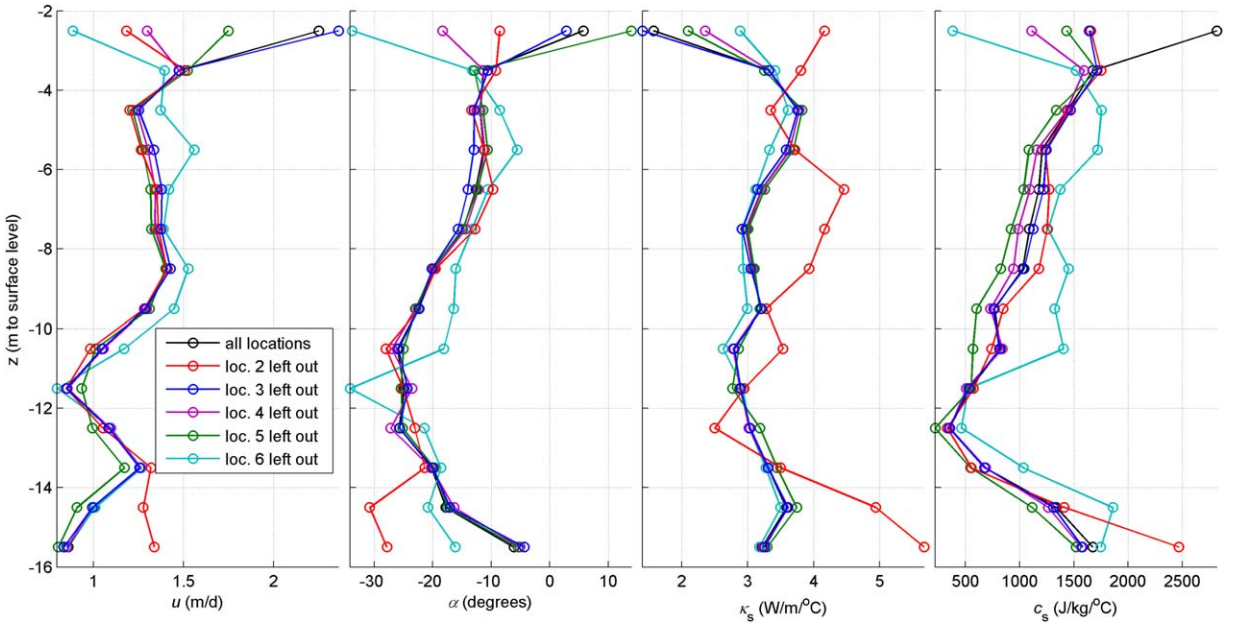

Figure 8. Optimal values of four parameters versus depth using temperature measurements at five locations (black line) or at four locations (see legend).

Results of the current analysis using temperature measurements along 5 cables are compared to the results of the analysis in the previous section where only the temperature measurements at the heating cable were used. Estimates of the magnitude of the velocity (triangles) and thermal conductivity of the solids (circles) of the current analysis are shown in Figure 6. The magnitude of the velocity is very similar for both analyses (except for the first meter below the water table, where estimates are inaccurate), including the dip in the velocity at a depth of 11 m. The values of the thermal conductivity κ_s of the solids are similar up to a depth of 10 m, below which the estimates with 5 cables are systematically lower than the estimates obtained in section 6.

An indication of the uncertainty of the fitted parameters is obtained by performing a leave-one-out bootstrap-type of analysis. The four parameters are estimated by using temperature measurements at 4 of the 5 locations, resulting in 5 additional estimates of the parameters. Together with the estimates using all 5 locations, this results in 6 estimates of the parameters sets, as shown in Figure 8. All 6 estimates are similar, which is an indication that the parameters can be estimated with reasonable certainty. The only exception is the first depth interval below the water table where parameters cannot be estimated accurately with the current model. The measurements at the heating cable (location 2) are important to estimate the thermal conductivity κ_s as leaving this measurement out gives significantly different values in an unrealistic range (red line); the optimal values of κ_s below a depth of 14 m are so unrealistic that the estimates of the other parameters are also unrealistic. Otherwise, the parameters u, α, and c_s are most sensitive to leaving out measurement 6 (light blue line). Measurements at location 6 are important as the location relative to the heating cable is fairly constant (Figure 7) and the cable is located in the general downstream direction of the heating cable.

8. Conclusions and Discussion

The insertion of fiber optic cables vertically into the ground with direct push equipment makes it possible to measure temperatures accurately and cost effectively over large depths in unconsolidated sedimentary aquifers. Temperature may be measured along fiber optic cables with a Distributed Temperature Sensing (DTS) unit. The main advantages of this method are that the inserted cables are in direct contact with the groundwater and aquifer material, the disturbance of the aquifer is minor, and no boreholes are needed. Installation with direct push equipment may be combined with a cone penetration test, which provides additional independent information about the aquifer material. Applications of the proposed technology includes both passive and active heat tracer tests.

An active heat tracer test consisting of six fiber optic cables and one heating cable was conducted to test the feasibility of the approach. Measurements of temperature change were used to determine the velocity of the groundwater. Realistic values were obtained with two different analyses, resulting in 7 different estimates of the parameters. Results of all analyses agreed reasonably well with each other and with the results of a cone penetration test, which was conducted when the fiber optic cables were installed.

The combined analysis of measurements at five fiber optic cables was complicated by the fact that the distance and orientation between the cables varied with depth. As the orientation and bending of the push rods was not measured during installation, the angle and orientation of each cable had to be estimated with an optimization procedure. The three-dimensional position of the cables must be measured in future applications of active heat tracer tests where multiple cables are installed close together to estimate velocities and subsurface parameters. The position of the steel rod (and thus the fiber optic cable) that is inserted into the ground can be measured very accurately with slope sensors, which are incorporated in modern drive points. In the presented methodology, the drive point remains in the ground, which makes the use of slope sensors rather expensive. Two solutions are envisioned. The first solution is to push and pull a drive point with slope sensors prior to inserting the fiber optic cable at every measurement location. It is likely that the drive point with the attached fiber optic cable will follow a similar path as the drive point with the slope sensors, especially when the truck isn't moved between the two penetrations. A more robust solution is to develop a device that contains the slope sensors and can store the measured slopes, but is not left behind in the ground with the fiber optic cables when the rods are pulled.

The analytic solution used to analyze the temperature measurements gives reasonable results for the fairly homogeneous aquifer where the active heat tracer experiment was conducted. Analysis of active heat tracer tests in more heterogeneous (layered) systems requires more sophisticated (numerical) solutions that take into account vertical heat exchange, buoyancy, and thermal dispersion. Similar models are required, including the effect of temperature on viscosity, for the analysis of passive heat tracer tests, which commonly take longer and cover larger areas.

In conclusion, the presented method of inserting fiber optic cables vertically into the ground with direct push equipment is a promising approach to measure temperature along vertical lines in unconsolidated sedimentary aquifers using DTS equipment. This cost-effective approach may create new opportunities to conduct passive and active heat tracer tests.

Acknowledgments
All temperature measurements are available from the authors upon request. This work was funded in part by a MIT-R&D collaboration grant within the cluster Watertechnology of the Topsector Water. The authors thank Nick van de Giesen, Koen Hilgersom, and Olivier Hoes from Delft University of Technology for their assistance with DTS equipment and the splicing of the fiber optic cables, and Ed Veling for his assistance with the solution to the heat transport equation. The assistance of Ed Rasenberg of PWN during the heat tracer experiments was greatly appreciated. This manuscript was improved by the reviews of Scott W. Tyler, Dave Hart, and an anonymous reviewer.

References

Acuña, J., P. Mogensen, and B. Palm (2011), Distributed thermal response tests on a multi-pipe coaxial borehole heat exchanger, *HVAC&R Res.*, *17*, 1012–1029.
Anderson, M. P. (2005), Heat as a ground water tracer, *Groundwater*, *43*, 951–968.
Becker, M. W., B. Bauer, and A. Hutchinson (2013), Measuring artificial recharge with fiber optic distributed temperature sensing, *Groundwater*, *51*, 670–678.
Briggs, M. A., L. K. Lautz, J. M. McKenzie (2012), A comparison of fibre-optic distributed temperature sensing to traditional methods of evaluating groundwater inflow to streams, *Hydrol. Processes*, *26*, 1277–1290.
Bristow, K. L., R. D. White, and G. J. Kluitenberg (1994), Comparison of single and dual probes for measuring soil thermal properties with transient heating, *Aust. J. Soil Res.*, *32*, 447–464.
Butler, J. J., J. M. Healey, G. McCall, E. J. Garnett, and S. P. Loheide (2002), Hydraulic tests with directpush equipment, *Groundwater*, *40*, 25–36.
Förster, A., J. Schrötter, D. F. Merriam, and D. D. Blackwell (1997), Application of optical-fiber temperature logging-An example in a sedimentary environment, *Geophysics*, *62*, 1107–1113.
Freifeld, B. M., S. Finsterle, T. C. Onstott, P. L. M. P. Toole, and L. M. Pratt (2008), Ground surface temperature reconstructions: Using in situ estimates for thermal conductivity acquired with a fiberoptic distributed thermal perturbation sensor, *Geophys. Res. Lett.*, *35*, L14309, doi:10.1029/2008GL034762.
Fujii, H., H. Okubo, K. Nishi, R. Itoi, K. Ohyama, and K. Shibata (2009), An improved thermal response test for U-tube ground heat exchanger based on optical fiber thermometers, *Geothermics*, *38*, 399–406.
Grosswig, S., E. Hurtig, and K. Kühn (1996), Fibre optic temperature sensing: A new tool for temperature measurements in boreholes, *Geophysics*, *61*, 1065–1067.
Hurtig, E., S. Grosswig, M. Jobmann, K. Kühn, and P. Marschall (1994), Fiber-optic temperature measurements in shallow boreholes: Experimental application for fluid logging, *Geothermics*, *23*, 355–364.
Keery, J., A. Binley, N. Crook, and J. W. Smith (2007), Temporal and spatial variability of groundwater-surface water fluxes: Development and application of an analytical method using temperature time series, *J. Hydrol.*, *336*, 1–16.
Kluitenberg, G. J., and A. W. Warrick (2001), Improved evaluation procedure for heat-pulse soil water flux density method, *Soil Sci. Soc. Am. J.*, *65*, 320–323.
Leaf, A. T., D. J. Hart, and J. M. Bahr (2012), Active thermal tracer tests for improved hydrostratigraphic characterization, *Groundwater*, *50*, 726–735.
Lebbe, L. C. (1999), *Hydraulic Parameter Identification*, Springer, N. Y.

Liu, G., S. Knobbe, and J. J. Butler (2013), Resolving centimeter-scale flows in aquifers and their hydrostratigraphic controls, *Geophys. Res. Lett.*, *40*, 1098–1103, doi:10.1002/grl.50282.
Lowry, C. S., J. F. Walker, R. J. Hunt, and M. P. Anderson (2007), Identifying spatial variability of groundwater discharge in a wetland stream using a distributed temperature sensor, *Water Resour. Res.*, *43*, W10408, doi:10.1029/2007WR006145.
Ma, R., C. Zheng, J. M. Zachara, and M. Tonkin (2012), Utility of bromide and heat tracers for aquifer characterization affected by highly transient flow conditions, *Water Resour. Res.*, *48*, W08523, doi:10.1029/2011WR011281.
Macfarlane, A., A. Förster, D. Merriam, J. Schrötter, and J. Healey (2002), Monitoring artificially stimulated fluid movement in the Cretaceous Dakota aquifer, western Kansas, *Hydrogeol. J.*, *10*, 662–673.
Mamer, E. A., and C. S. Lowry (2013), Locating and quantifying spatially distributed groundwater/surface water interactions using temperature signals with paired fiber-optic cables, *Water Resour. Res.*, *49*, 7670–7680, doi:10.1002/2013WR014235.
Moffett, K. B., S. W. Tyler, T. Torgersen, M. Menon, J. S. Selker, and S. M. Gorelick (2008), Processes controlling the thermal regime of salt-marsh channel beds, *Environ. Sci. Technol.*, *42*, 671–676.
Mori, Y., J. W. Hopmans, A. P. Mortensen, and G. J. Kluitenberg (2005), Estimation of vadose zone water flux from multi-functional heat pulse probe measurements, *Soil Sci. Soc. Am. J.*, *69*, 599–606.
Rau, G. C., M. S. Andersen, A. M. McCallum, and R. I. Acworth (2010), Analytical methods that use natural heat as a tracer to quantify surface water-groundwater exchange, evaluated using field temperature records, *Hydrogeol. J.*, *18*, 1093–1110.
Read, T., O. Bour, V. Bense, T. Le Borgne, P. Goderniaux, M. V. Klepikova, R. Hochreutener, N. Lavenant, and V. Boschero (2013), Characterizing groundwater flow and heat transport in fractured rock using fiber-optic distributed temperature sensing, *Geophys. Res. Lett.*, *40*, 2055–2059, doi:10.1002/grl.50397.
Ren, T., G. J. Kluitenberg, and R. Horton (2000), Determining soil water flux and pore water velocity by a heat pulse technique, *Soil Sci. Soc. Am. J.*, *64*, 552–560.
Sayde, C., C. Gregory, M. GilRodriguez, N. Tufillaro, S. Tyler, N. van de Giesen, M. English, R. Cuenca, and J. S. Selker (2010), Feasibility of soil moisture monitoring with heated fiber optics, *Water Resour. Res.*, *46*, W06201, doi:10.1029/2009WR007846.
Selker, J. S., L. Thevenaz, H. Huwald, A. Mallet, W. Luxemburg, N. van de Giesen, M. Stejskal, J. Zeman, M. Westhoff, and M. B. Parlange (2006), Distributed fiber-optic temperature sensing for hydrologic systems, *Water Resour. Res.*, *42*, W12202, doi:10.1029/2006WR005326.
Shampine, L. F. (2008), Vectorized adaptive quadrature in MATLAB, *J. Comput. Appl. Math.*, *211*, 131–140.
Steele-Dunne, S. C., M. M. Rutten, D. M. Krzeminska, M. Hausner, S. W. Tyler, J. Selker, T. A. Bogaard, and N. C. van de Giesen (2010), Feasibility of soil moisture estimation using passive distributed temperature sensing, *Water Resour. Res.*, *46*, W03534, doi:10.1029/2009WR008272.
Striegl, A. M., and S. P. Loheide II (2012), Heated distributed temperature sensing for field scale soil moisture monitoring, *Groundwater*, *50*, 340–347.
Tyler, S. W., J. S. Selker, M. B. Hausner, C. E. Hatch, T. Torgersen, C. E. Thodal, and S. G. Schladow (2009), Environmental temperature sensing using Raman spectra DTS fiber-optic methods, *Water Resour. Res.*, *45*, W00D23, doi:10.1029/2008WR007052.
van de Giesen, N., S. C. Steele-Dunne, J. Jansen, O. Hoes, M. B. Hausner, S. Tyler, and J. Selker (2012), Double-ended calibration of fiber-optic Raman spectra distributed temperature sensing data, *Sensors*, *12*, 5471–5485.
Vandenbohede A., A. Louwyck, and L. Lebbe (2009), Conservative solute versus heat transport in porous media during push-pull tests, *Transp. Porous Media*, *76*, 265–287.
Veling, E. J. M., and C. Maas (2010), Hantush well function revisited, *J. Hydrol.*, *393*, 381–388.
Verruijt, A. (2012), *Soil Mechanics*. [Available at http://geo.verruijt.net/software/SoilMechBook2012.pdf.]
Vogt, T., P. Schneider, L. Hahn-Woernle, and O. A. Cirpka (2010), Estimation of seepage rates in a losing stream by means of fiber-optic high-resolution vertical temperature profiling, *J. Hydrol.*, *380*, 154–164.
Wagner, V., P. Blum, M. Kübert, and P. Bayer (2013), Analytical approach to groundwater-influenced thermal response tests of grouted borehole heat exchangers, *Geothermics*, *46*, 22–31.
Wagner, V., T. Li, P. Bayer, C. Leven, P. Dietrich, and P. Blum (2014), Thermal tracer testing in a sedimentary aquifer: Field experiment (Lauswiesen, Germany) and numerical simulation, *Hydrogeol. J.*, *22*, 175–187.
Westhoff, M. C., H. H. G. Savenije, W. M. Luxemburg, G. S. Stelling, N. C. van de Giesen, J. S. Selker, L. Pfister, and S. Uhlenbrook (2007), A distributed stream temperature model using high resolution temperature observations, *Hydrol. Earth Syst. Sci.*, *11*, 1469–1480.
Zubair, S. M., and M. A. Chaudhry (1996), Temperature solutions due to time-dependent moving-line-heat sources, *Heat Mass Transfer*, *31*, 185–189.